



Apparent optical properties of the Canadian Beaufort Sea – Part 2: The 1 % and 1 cm perspective in deriving and validating AOP data products

S. B. Hooker¹, J. H. Morrow², and A. Matsuoka³

¹NASA Goddard Space Flight Center, Ocean Ecology Laboratory, Greenbelt, Maryland 20771, USA

²Biospherical Instruments Inc., 5340 Riley Street, San Diego, California 92110, USA

³Université Laval, Avenue de la Médecine, Québec City, QC G1V 0A6, Canada

Correspondence to: S. B. Hooker (stanford.b.hooker@nasa.gov)

Received: 29 March 2012 – Published in Biogeosciences Discuss.: 27 July 2012

Revised: 30 January 2013 – Accepted: 30 March 2013 – Published: 4 July 2013

Abstract. A next-generation in-water profiler designed to measure the apparent optical properties (AOPs) of seawater was developed and validated across a wide dynamic range of in-water properties. The new free-falling instrument, the Compact-Optical Profiling System (C-OPS), was based on sensors built with a cluster of 19 state-of-the-art microradiometers spanning 320–780 nm and a novel kite-shaped *backplane*. The new backplane includes tunable ballast, a *hydrobaric* buoyancy chamber, plus pitch and roll adjustments, to provide unprecedented stability and vertical resolution in near-surface waters. A unique data set was collected as part of the development activity plus the first major field campaign that used the new instrument, the Malina expedition to the Beaufort Sea in the vicinity of the Mackenzie River outflow. The data were of sufficient resolution and quality to show that errors – more correctly, uncertainties – in the execution of data sampling protocols were measurable at the 1 % and 1 cm level with C-OPS. A theoretical sensitivity analysis as a function of three water types established by the peak in the remote sensing reflectance spectrum, $R_{rs}(\lambda)$, revealed which water types and which parts of the spectrum were the most sensitive to data acquisition uncertainties. Shallow riverine waters were the most sensitive water type, and the ultraviolet and near-infrared spectral *end members*, which are critical to next-generation satellite missions, were the most sensitive parts of the spectrum. The sensitivity analysis also showed how the use of data products based on band ratios significantly mitigated the influence of data acquisition uncertainties. The unprecedented vertical resolution provided

high-quality data products, which supported an alternative classification capability based on the spectral diffuse attenuation coefficient, $K_d(\lambda)$. The $K_d(320)$ and $K_d(780)$ data showed how complex coastal systems can be distinguished two-dimensionally and how near-ice water masses are different from the neighboring open ocean. Finally, an algorithm for predicting the spectral absorption due to colored dissolved organic matter (CDOM), denoted $a_{CDOM}(\lambda)$, was developed using the $K_d(320)/K_d(780)$ ratio, which was based on a linear relationship with respect to $a_{CDOM}(440)$. The robustness of the approach was established by expanding the use of the algorithm to include a geographically different coastal environment, the Southern Mid-Atlantic Bight, with no significant change in accuracy (approximately 98 % of the variance explained). Alternative spectral end members reminiscent of next-generation (340 and 710 nm) as well as legacy satellite missions (412 and 670 nm) were also used to accurately derive $a_{CDOM}(440)$ from $K_d(\lambda)$ ratios.

1 Introduction

A number of international ocean color satellite sensors have been designed and launched in the last decade and a half to support oceanographic studies and applications including the following: the Ocean Color and Temperature Scanner (OCTS), the Sea-viewing Wide Field-of-view Sensor (SeaWiFS), two Moderate Resolution Imaging Spectroradiometer (MODIS) instruments, and the Medium Resolution

Imaging Spectrometer (MERIS). These *legacy* sensors have contributed to the general problem of inverting optical measurements to derive concentration estimates of biogeochemical parameters, and some continue to provide regular coverage of the global biosphere. The SeaWiFS and MODIS missions are of particular importance because their calibration and validation capabilities were developed in parallel and established many of the requirements for ocean color research, e.g., the atmospheric correction scheme. A notable joint accomplishment was creating a separate site for vicarious calibration, which involved a rotating deployment of custom-built Marine Optical Buoy (MOBY) units in a clear-water site (Clark et al., 1997).

Worldwide deployments of commercial off-the-shelf (COTS) radiometers are a primary source of algorithm validation data for ocean color data products, because they are one of the few mechanisms to sample the dynamic range involved. The SeaWiFS Bio-optical Archive and Storage System (SeaBASS) has provided long-term access to these data for the global community (Hooker et al., 1994). COTS instruments have also been used for vicarious calibration, which is primarily an open-ocean problem because of the need for spatial and temporal homogeneity during data acquisition, at a similar level of efficacy to custom hardware like MOBY (Bailey et al., 2008). The ability to use COTS hardware for vicarious calibration was also confirmed by the *Bouée pour l'acquisition de Séries Optiques à Long Terme* (BOUSOLE) project (Antoine et al., 2008). The central theme in the discussion presented here is the incremental pursuit of more-accurate field observations, at the 1 % level normally associated with vicarious calibration, while ensuring access to state-of-the-art advances by making the solutions commercially available.

The current challenge in ocean color remote sensing is to extend the open-ocean accomplishments into much shallower waters (McClain et al., 2006), e.g., estuaries and rivers. This requirement is driven by the present focus of satellite observations, which are inexorably tied to launching new missions based on novel research topics and ensuring the quality of the ensuing satellite data. The long-term NASA programmatic requirements for ocean color remote sensing span a range of scales and applications (Hooker et al., 2007): (a) global separation of pigments and ecosystem components, (b) high spatial and temporal resolution of near-shore waters, (c) active assessment of plant physiology and composition, and (d) determination of mixed layer depths. The corresponding programmatic research questions span equally large scales: how oceanic ecosystems and their attendant biodiversity are influenced by environmental changes and how they evolve over time; how carbon transitions between oceanic pools and passes through the Earth system; and how the diversity and distribution of coastal marine habitats change. These inquiries require more-interdisciplinary science and greater numbers of high-accuracy observations in the land–sea boundary, because the types and diversity of

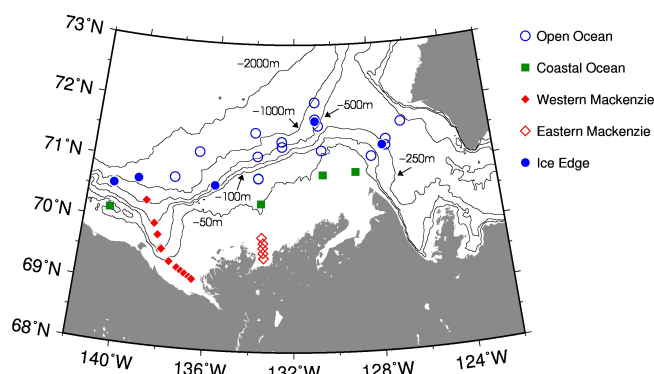


Fig. 1. The location of Malina optical stations color coded to show the western and eastern Mackenzie transects (red solid and open diamonds, respectively), open-ocean and ice-edge stations (blue open and solid circles, respectively), and coastal stations (green squares).

data products involve more optically complex waters than the legacy perspective.

A case study applicable to the aforementioned research questions is the Malina campaign, which was undertaken in the 2009 Boreal summer (August) to the Canadian Arctic within the vicinity of the Mackenzie River outflow in the Beaufort Sea. A central Malina objective is to understand the fate of terrestrial carbon exported to the Arctic Ocean, which means the optical characterization of riverine source waters and their subsequent evolution – e.g., settling, mixing, and photo-oxidation – in the near-shore environment was anticipated to be important during the planning of the fieldwork. Aspects of this objective provided the motivation for the characterization of the water masses and the derivation of water constituents from the optical data (discussed below), as well as how the sampling was pursued and the optical stations classified. As shown in Fig. 1, classification was based on whether data were obtained in the open ocean, near the (moving) ice edge, within the Mackenzie River plume, or in coastal waters.

Another objective of the results presented here is to initiate the preparedness for the next-generation of ocean color satellites (NRC, 2007; NASA, 2010) with the most capable COTS instrumentation in the shortest time possible while providing baseline results of optically complex coastal waters to contribute to the underlying science questions associated with NASA programs and mission offices. The optical data set is expected to provide the science teams with high-quality data that can be used to start formulating and testing the myriad details associated with hypotheses, algorithms, and databases for the new missions. Because of the emphasis on the near-shore environment, which is typified by shallow water depths and an optically complex vertical structure, there is the added requirement to demonstrate that the new technology can be validated in waters with unprecedented multi-dimensional heterogeneity.

2 Background

The principal data product in ocean color research is the radiant energy emerging from the sea, the so-called *water-leaving radiance*, $L_W(\lambda)$, where λ denotes wavelength. For the purposes of ground truth – more correctly, *sea-truth* – observations, $L_W(\lambda)$ can be derived by extrapolating in-water measurements taken close to the sea surface or obtained directly from above-water measurements. For meaningful applications, an extremely high radiometric accuracy is required. The SeaWiFS Project, for example, established a radiometric accuracy to within 5 % absolute and 1 % relative, and chlorophyll *a* concentration to within 35 % over a range of 0.05–50.0 mg m⁻³ (Hooker and Esaias, 1993). Variables explicitly accounting for the global solar irradiance, $E_d(0^+, \lambda)$, at the time of data collection – so-called apparent optical properties (AOPs) – are used for matchup analysis, because derivations of $L_W(\lambda)$ in identical waters, but different illumination conditions, will differ.

Commercial systems capable of measuring in-water AOPs in the open ocean with an accuracy in keeping with calibration and validation requirements were refined during the preparation and launch of SeaWiFS and the two MODIS instruments (Hooker and Maritorena, 2000). Some commercial instruments were shown to be acceptable in turbid coastal waters and atmospheres under restricted circumstances (Hooker et al., 2004). Above-water methods were particularly appropriate for coastal waters, because they did not have to resolve the vertical complexity of the water column, which in coastal waters typically involves one or more optically different layers close to the surface (Hooker et al., 2002). Another advantage of the above-water approach was being able to expand it to include atmospheric measurements with the same instrumentation (Hooker et al., 2000), which are important in coastal validation exercises. Problems associated with platform perturbations associated with above-water sensor systems were shown to be solvable (Hooker and Zibordi, 2005), which permitted a networked capability of above-water radiometers for remote sensing validation in coastal waters (Zibordi et al., 2004). The development of a telescoping mast for deploying solar technologies with unobstructed viewing (Hooker, 2010) has virtually eliminated platform contamination of upward and downward above-water observations (Hlaing et al., 2010). In-water profiles are nonetheless needed, because of what they reveal about light penetration, and because not all AOP parameters can presently be obtained directly from an above-water method, e.g., the spectral diffuse attenuation coefficient, $K_d(\lambda)$, the importance of which is presented below.

The legacy perspective for remote sensing has focused on the open ocean (Hooker and McClain, 2000), because the missions were designed around the fact that the majority of the oceanic pixels in a global image are barren. The relative simplicity of clear waters means the so-called *case-1* optical properties are solely determined by the phytoplankton and

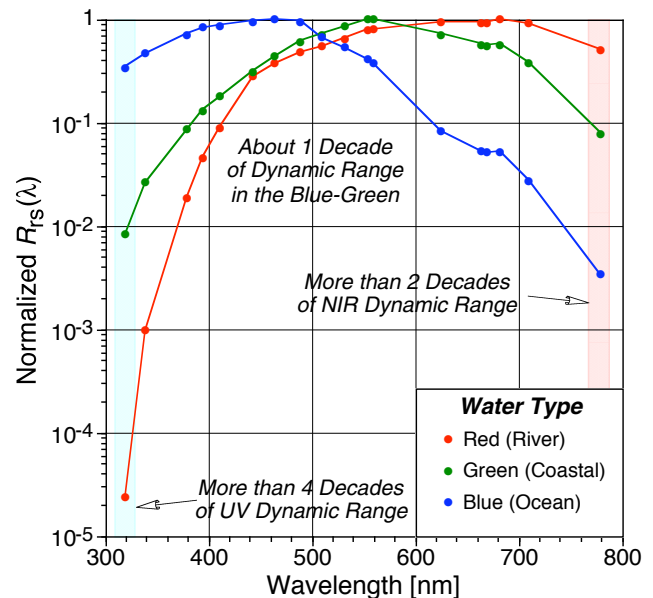


Fig. 2. Averaged Malina $R_{rs}(\lambda) = L_W(\lambda)/E_d(0^+, \lambda)$ spectra, normalized by the peak value of the spectrum. The spectra are separated into three groups based on the peak wavelength domain (blue, green, and red) and classified as river, coastal, or ocean based on the preponderance of the sampling locations.

their derivative products (Morel and Prieur, 1977), whereas for turbid case-2 waters they are not. Case-1 waters do not require an extensive set of spectral bands for high-quality data products, which rely primarily on the blue-green visible (VIS) wavelengths. Although Arctic AOPs were recognized as different than the world ocean used to derive global satellite data products (Cota et al., 2004), the results presented below show that Arctic AOPs are more complex than first established, in part because early studies in these same areas were spectrally restricted. Wang and Cota (2003), for example, used VIS data, so ultraviolet (UV) and near-infrared (NIR) properties could only be inferred. A single-instrument architecture with the necessary spectral and sampling resolution to span the dynamic range of near-shore turbid waters and atmospheres to open-ocean blue waters and skies was not needed for the VIS legacy perspective. The Fig. 2 Malina spectra, collected with a new optical instrument discussed below, show that the dynamic range in the blue-green domain is at a minimum as a function of the water types encountered in the Beaufort Sea. The greatest dynamic range occurs in the UV and NIR spectral *end members*, and offer the greatest opportunity – with a sensitivity caution – for deriving seawater constituents (discussed below).

Although free-falling, but tethered, in-water profilers can be floated away to avoid platform perturbations associated with the structure from which the instrumentation is being deployed (e.g., a research vessel), additional problems remain and are a function of the basic design. Rocket-shaped

profilers use buoyant fins and a weighted *nose* to vertically orient the light sensors, but, regardless of their length, a rather high descent speed is needed to maintain vertical stability to within reasonable thresholds (usually to within 5°). Close to the surface, when the righting moment associated with releasing the profiler is established, large oscillations are common and much of the near-surface data are unusable. In a developed sea state with swell and wind waves, the oscillations can be accentuated, and the first depths of usable data can be as deep as 3–5 m, depending on how the light sensors are mounted on the profiler. In addition to the depth for usable data, there is also the practical problem that an instrument that is approximately 1 m or more in length and descending on the order of $0.6\text{--}1.0\text{ ms}^{-1}$ is very difficult to use in a 2–5 m deep river.

The significance of acquiring high-quality optical data close to the sea surface is expressed directly in the processing scheme used to derive the data products. The processor used here is based on a well-established methodology (Smith and Baker, 1984) that Hooker et al. (2001) showed was capable of agreement at the 1 % level within an international round robin, when the processing options were as similar as possible. This level of achievement is only possible if the acquisition and processing of the data strictly adheres to the NASA Ocean Optics Protocols (hereafter, the Protocols). The Protocols used Joint Global Ocean Flux Study (JGOFS) sampling procedures (JGOFS, 1991) to initially set the standards for calibration and validation activities (Mueller and Austin, 1992), which were revised (Mueller and Austin, 1995) and updated over time (Mueller, 2000, 2002, 2003). Details of the data processing scheme (Hooker and Brown, 2013) are summarized in the companion paper (Antoine et al., 2013).

2.1 Next-generation perspective

The emphasis on coastal processes in next-generation planning created a potential void in the instrumentation needed to provide sea-truth observations at the necessary quality level. Although existing above-water sensors could provide the needed L_W measurements directly, they could not provide the desired water column properties. Existing free-falling in-water instruments could provide the latter, but not always close to the sea surface and not always at the desired vertical resolution, because they were long devices (1 m in length or more) that fell quickly (about 1 ms^{-1}) with a slow data rate (usually 6 Hz). Adding to the difficulty with a legacy approach was that slowing the descent rate of a rocket-shaped profiler usually led to high data losses from excessive vertical tilts (data that is not planar to within 5° are rejected when deriving L_W).

An in-water alternative was to mount the light sensors in a winch-and-crane system, but such an approach has difficulty making unperturbed measurements close to the sea surface, because of the presence and motion of the ship or deployment platform except under specialized circumstances

(Zibordi et al., 2002). There was also the need to reduce the size of the sensors to minimize self-shading effects (important in turbid waters) and to make alternative deployment platforms more accessible (e.g., remotely or autonomously piloted vehicles) to expand the total number of observations being submitted to databases. What was needed was smaller light sensors with faster sampling rates that could be mounted on a new *backplane* that held the sensors and stably fell through the water very slowly. The resulting high vertical resolution would allow the optical complexity of water masses to be resolved. That is, thin intrusive layers (perhaps of freshwater origin from rivers or melting ice) would be properly sampled for the first time in a freely falling package, as would the rapid light variations in clear open-ocean waters. Both these complexities were usually aliased in the sampling by legacy devices. To promote international partnerships, a COTS solution available to worldwide researchers was attractive. The basic design criterion was a Compact-Optical Profiling System (C-OPS) that was equally capable of sampling shallow (2 m) rivers and the open ocean (200 m).

The first step in developing a new free-falling profiler was to enhance a COTS radiometer as the starting point for testing new design concepts in the laboratory and field. The Biospherical Surface Ocean Reflectance System (BioSORS), an above-water system manufactured by Biospherical Instruments Inc. (San Diego, California) with 19 wavebands, was used to test the new size reduction and characterization concepts while retaining an approximately 10-decade range in responsivity (Hooker et al., 2010a). The latter was critical to the new approach, because an anticipated above-water application of the new technology was to support joint ocean–atmosphere remote sensing, like the next-generation Aerosol–Cloud–Ecosystems (ACE) and Pre-Aerosol, Clouds, and Ocean Ecosystem (PACE) missions (NASA, 2010). A common architecture for both above- and in-water instruments was imagined, because this would reduce costs and make the new COTS technology more accessible for the global research community.

For next-generation missions, it was anticipated that a more sophisticated above-water version of the new sensor system would function as a radiometer to sample the ocean and as a sun photometer to sample the atmosphere (Hooker et al., 2012). Such a capability had already been established with a commercial sun photometer (Hooker et al., 2000) with a small number of VIS channels, but a more capable system with polarization and a larger spectral range from the UV to the short-wave infrared (SWIR) was needed for next-generation missions. At this early stage, the design had to include a hyperspectral component to support missions like the Geostationary Coastal and Air Pollution Events (GEOCAPE) and the Hyperspectral Infrared Imager (HyspIRI). Next-generation missions place an emphasis on high-quality UV and NIR data products. These spectral end members pose a significant problem for in-water data acquisition because the signals are usually highly attenuated (Fig. 2) and must be

accurately recorded very close to the sea surface, which is a source of degrading perturbations. Consequently, the next critical stage was associated with the unique aspects of the use of the sensors as part of an in-water profiler.

3 A kite-shaped profiler

The lessons learned with the BioSORS sensors were incorporated into a new in-water profiler called the Biospherical Profiler (BioPRO), a 19-channel (λ_{19}) device based on an established rocket-shaped design, although the fins were not buoyant (Hooker et al., 2010b). Open-ocean deployments of BioPRO showed the sensor modifications to date resulted in excellent performance with respect to the standards at the time. An open-ocean (case-1) intercomparison with a legacy instrument based on common wavelengths showed that the unbiased percent difference (UPD¹) for each channel between the two profilers averaged -7.6% to 0.3% , with an overall average of -2.2% , which is to within the calibration uncertainty. The largest difference corresponded to the 510 nm channel, which was a source of bias and a problematic wavelength with a particular class of legacy radiometers (Hooker and Maritorena, 2000). A least-squares linear regression of the data showed almost one-to-one correspondence to within 4.2% , with over 99 % of the variance explained, and a root mean square error (RMSE) of 1.8% .

The follow-on Submersible Biospherical Optical Profiling System (SuBOPS) combined the incremental changes in radiometry with a compact backplane for mounting the light sensors that could descend more slowly while also very stably (Hooker et al., 2010b). The new backplane used a four-point harness reminiscent of a kite. The orientation of the light sensors could be quickly adjusted to counter cable tension (or an in situ current), and movable flotation allowed the light sensors to be *trimmed* to maintain a planar geometry. One or more compressible *air bladders* contained within a floodable *hydrobaric* buoyancy chamber allowed the instrument to loiter at the sea surface before descending and reaching terminal velocity, which greatly improved near-surface vertical resolution.

With respect to a legacy profiler, SuBOPS recorded greater than a factor of 10 more samples in the near-surface 5, 10, and 15 m of the water column. SuBOPS had a vertical sampling resolution of approximately 1 cm in the upper 5 m and captured the high-frequency perturbations associated with wave-focusing effects, thereby minimizing the aliasing normally encountered with legacy devices. The adjustable features of the new backplane maintained the planar orientation of the light sensors to within 5° except during significantly adverse conditions. To focus on improving coastal ob-

servations, the SuBOPS and BioPRO intercomparisons were in eutrophic (case-2) waters. The average UPD for channels common to the first BioPRO intercomparison ranged from -3.5% to 3.6% , with an overall average of 1.3% , which is to within the calibration uncertainty. A least-squares linear regression of the data showed one-to-one correspondence to within 4.0% , with over 96 % of the variance explained, and an RMSE of 4.5% .

Following an incremental approach to manage risk, the next improvement used new radiometers that were emerging from a development activity based on *microradiometers* (Booth et al., 2010). The microradiometer approach established – for the first time in oceanographic optical instrumentation – a single-instrument design with inherent flexibility and dynamic range as to be scalable across all the sampling requirements for both above- and in-water AOP measurements (Morrow et al., 2010a). A microradiometer has components so small that they must be machine assembled. The outer diameter of 1.1 cm is set by the photodetector, and after the fore optics and metal shielding are applied the overall length is 9.6 cm. Automated production with conformal coating of the electronics removed almost all of the instrument-to-instrument performance variability that had plagued hand-made legacy instruments.

In practice, system expansion for a radiance sensor built with microradiometers is only limited by data rates, because each microradiometer, after application of the fore-optics, is a fully functional radiance sensor. Irradiance sensors are more constrained, because each microradiometer has to properly view the solitary diffuser used in the construction of the cosine collector. The 21.4 % smaller size of the C-OPS housings, and the rigid, linear form factor of microradiometers, posed challenges. For multiple-waveband instruments, the length of individual microradiometers meant they could not be tilted to orient them at the center of the secondary diffuser and still maintain a small sensor diameter. To solve this problem, a plano-convex lens was developed to control the viewing geometry and center each microradiometer on the same area of the lower intermediate diffuser (Booth et al., 2010).

4 C-OPS commissioning and intercomparisons

The first C-OPS realization of the original free-falling design concept combined all the lessons learned to date into a single device (Morrow et al., 2010b). Part of the attraction of sensor systems built from microradiometers includes their adaptability to sensor networking, for example, acquiring data from an ancillary sensor like a global positioning system (GPS) device or controlling an accessory such as a shadowband attachment for the solar reference (Bernhard et al., 2010). The latter can be used to improve the self-shading correction by providing measurements of the sky irradiance. Figure 3 presents the C-OPS instrument in its

¹The UPD is defined as $200(Y - X)/(Y + X)$, where X is the reference data (in this case the legacy profiler), but the other data are equally valid. UPD statistics are used here to discern biases, which should not be present.

most advanced state including the use of a custom-blended, low-density polyurethane resin for buoyancy, which was specially formulated to produce a rigid foam that is machinable while retaining a very high crush and water resistance.

The C-OPS instrument was commissioned in mesotrophic (case-1) coastal waters and evaluated in eutrophic (case-2) coastal waters by intercomparing it with the SuBOPS instrument (Morrow et al., 2010b). The intercomparisons included above- and in-water trials because the C-OPS solar reference was a new design involving a plano-convex lens. The average unbiased percent difference for a subset of nine channels between the two in-water systems ranged from -7.0% to 6.5% , with an overall average of 1.8% (case-1) and -0.8% (case-2), which is to within the calibration uncertainty. A least-squares linear regression of the data showed one-to-one correspondence to within 2.0% for both water types, with 97% or more of the variance explained, and RMSE values to within 4.8% . The solar references had a UPD range of -2.5% to 3.9% , with an overall average of 1.3% (for the same wavelengths as the in-water results), which is also to within the calibration uncertainty. A least-squares linear regression of the data showed one-to-one correspondence to within 4.5% , with over 99% of the variance explained, and an RMSE value of 2.1% .

With the addition of the UV and NIR end members to the intercomparisons, the UPD range increases and reaches -50.7% at 780 nm . This increase is caused by the presence of near-surface layers in the case-2 environment. Although the two profilers were very similar in their capabilities (e.g., both had vertical tilts to within 1.5°), C-OPS had the most advanced backplane, which allowed longer duration surface loitering. Consequently, more C-OPS data were collected in the part of the water column that was the most sensitive to differences in vertical sampling resolution. The difference in surface loitering resulted in the C-OPS extrapolation intervals having almost 70% more data than SuBOPS when near-surface layers were present. For highly attenuated wavelengths, this exposed an important difference between the two profilers and created the concept of estimating the degradation in producing data products from profiles wherein the data sampling was not in keeping with the optical complexity of the water column as a function of wavelength. The fact that the validation intercomparisons were successfully conducted in the most challenging (case-2) waters demonstrated that AOP measurements could be validated across a wide dynamic range in water properties and suggested that the sensitivities for all spectral domains to sampling resolution problems could potentially be investigated in the field with a single high-resolution instrument (C-OPS).

5 The 1 % and 1 cm perspective

To partition the dynamic range, the AOP profiles are separated into three groups based on the peak in the remote sens-

ing reflectance, $R_{rs}(\lambda)$, spectrum (Fig. 2): blue, green, and red, with the latter used if the peak is in the NIR domain. These respective categories correspond to deep oceanic, shallow coastal, and very shallow riverine waters (Fig. 1). The C-OPS instrument was deployed from the so-called *barge* during the Malina campaign within these three categories of water types, and it was used to collect data close to the ice edge on several occasions. Because C-OPS was deployed from a small vessel launched from an icebreaker, the majority of the sampling was in undisturbed waters, wherein the small boat drifted into the sampling area. The proximity of the ice or sampling in the Mackenzie River plumes ensured the majority of the data were obtained in areas with limited fetch and rather calm sea surfaces. Only 9 casts out of 148 were collected under clear-sky conditions with the rest under overcast, so wave-focusing effects were minimal.

The relatively calm surface conditions resulted in near-planar observations throughout the water column with average vertical tilts in the extrapolation interval being less than 2.5° . The quiet conditions permitted slow descent velocities of $6\text{--}12\text{ cm s}^{-1}$ near the surface, with the slowest speeds in the Mackenzie River. Because the profiler samples at 12 Hz , the nominal vertical resolution of C-OPS sampling in the upper 5 m of the water column was 1 cm or less. The number of points retained in the extrapolation interval after applying a 5° tilt exclusion criteria ranged from 95 to 183 for E_d and from 74 to 176 for L_u (the L_u aperture is displaced below the E_d aperture). Two extrapolation intervals were used, one for the blue-green and UV wavelengths, and a separate one for the red and NIR wavelengths. Both intervals started at the same depth, but the former was allowed to extend below the latter if water column homogeneity permitted. The extrapolation depth interval ranged from $1.0\text{--}2.4\text{ m}$ and averaged about 1.5 m .

The high vertical resolution achieved with the C-OPS instrument is based on the following: (a) the number of samples recorded per meter of near-surface depth (about 175), (b) the number of observations retained per meter of extrapolation interval (approximately 95 on average), and (c) the capabilities of the pressure transducer. All three of these performance metrics support an approximately 1 cm (or better) vertical resolution in the optical fields and allow well-resolved theoretical sensitivity analyses to be performed on a variety of deployment practices that can degrade the quality of the observations and, thus, the data products derived from the data. Of the three sources of vertical resolution, the pressure transducer is common to all three, because it defines the vertical extent of the sampling and the instantaneous location of the profiler in the water column. The C-OPS instrument uses a compensated piezoresistive silicon pressure sensor packaged in a 316L stainless steel housing. The nonlinearity, repeatability, hysteresis, and long-term stability of the pressure sensor all contribute to the accuracy and precision of the recorded depth. Based on repeated calibrations and laboratory experiments, the upper 5 m of the near-surface water

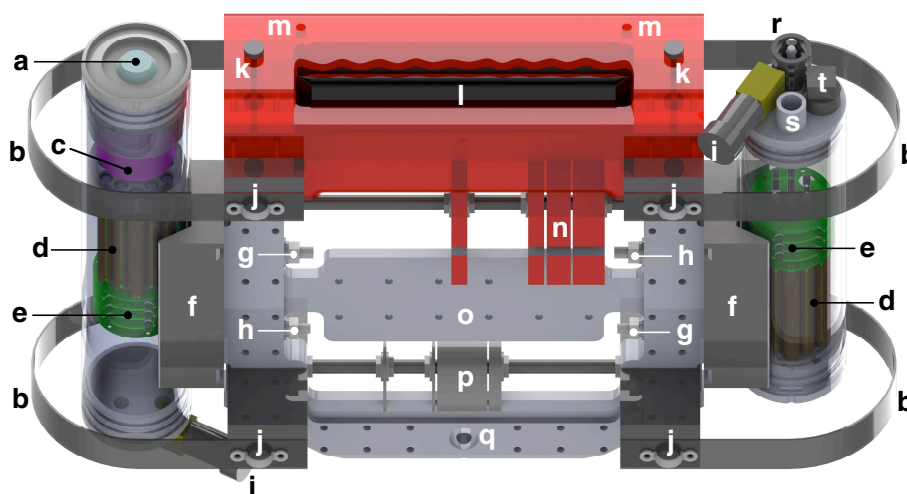


Fig. 3. A transparent drawing of the C-OPS in-water instrument showing the following components (the *roll* axis is along the long axis of the instrument and the *pitch* axis is along the short axis, which is into or out of the page): (a) the cosine collector for the irradiance sensor; (b) the *bumpers*, which protect the light sensors from side impacts during deployment and recovery; (c) the irradiance lens, which uniformly spreads the diffuse light from the cosine collector out across the array of microradiometer apertures below the lens; (d) the cluster of 19 microradiometers; (e) the aggregator and support electronics boards, which allow the microradiometers to be controlled as a single device; (f) the sensor v-blocks, which are attached to the backplane at a fixed point and a rotation point; (g) the fixed point nuts; (h) the pitch adjustment nuts, which when loosened allow an offset bias of the sensor to be set to counter cable tension or an ambient current that can pitch the instrument away from the desired vertical tilt of less than 5°; (i) the dummy plugs attached to the sensor bulkhead connectors (cabling not shown for clarity); (j) the harness attachment points (harness not shown for clarity); (k) the knurled screws that hold the lid on the hydrobaric buoyancy chamber, which can contain a mix of up to three compressible bladders and rigid foam inserts; (l) the hydrobaric buoyancy chamber revealed with the use of a cutaway section to have two air-filled bladders, which slowly compress and allow the instrument to loiter near the sea surface; (m) the air holes that allow the hydrobaric buoyancy chamber to flood (two of four shown); (n) the foam flotation disks, which can be moved from side to side to trim the roll axis of the instrument to maintain a desired vertical tilt of less than 5° (the slotted edge is visible as the dark band below the letter “n” for clarity, but is normally oriented downwards and then held tightly by the nuts to the left and right of the disks); (o) the perforated backplane (the holes allow for securing the cabling and the mounting of other devices); (p) the weight disks, which like the flotation disks are slotted and firmly affixed using nuts to the left and right, establish the negative buoyancy and can be moved from side to side to trim the roll axis of the instrument; (q) the fitting point for a flexible or rigid downward-pointing spar, which if used can provide protection against a bottom impact; (r) the water temperature probe; (s) the pressure transducer port; and (t) the nitrogen purge fitting (one on each sensor).

column is expected to have a pressure reading accuracy to within 0.5 mm and a precision to within 0.1 mm.

A number of additional factors need to be considered when working in aquatic systems for near-surface measurements, but they are often overlooked or underappreciated. Those related to the transducer, such as temperature coefficients of scale and offset, can be addressed by careful design and *taring* of the pressure measurement as part of the measurement protocol. It is also important to deploy the instrument correctly to minimize the effect of hysteresis and to maintain the instrument in a thermal condition similar to the waters to be sampled. When the instrument is deployed, circular motions near the surface impose different accelerations on the instrument in the wave field. Deconvolving the pressure reading produced by the inertia of the diaphragm and media in the pressure cavity from the actual pressure reading caused by the vertical water column is an area of continuing investigation. For the Malina campaign, the majority of the deploy-

ments were in relatively quiescent waters where these effects were minimized.

The first theoretical sensitivity analysis considered here is the influence of artificial vertical displacements on the data. An example source for such a displacement would be incorrectly determining the offset distance between the light sensor aperture and the pressure transducer (Fig. 3). Calibration and validation uncertainties require this type of uncertainty, as measured by the relative percent difference (RPD²), to be unbiased and less than 1 %.

²The RPD is defined as $100(Y - X)/X$, where X is the reference data (no artificial vertical displacement) and is used here to show the level of bias, which should be present, once an artificial displacement is applied to Y .

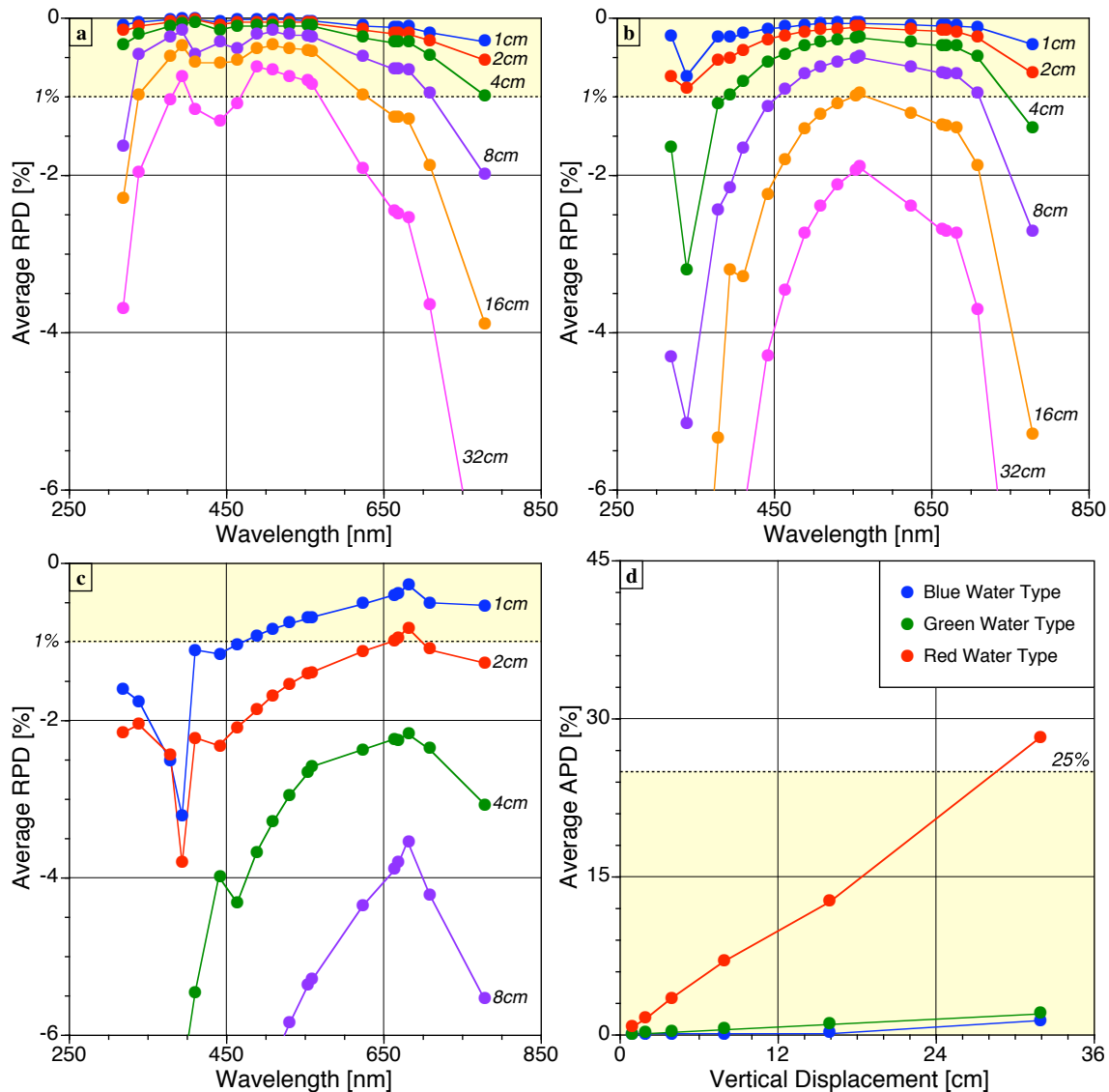


Fig. 4. The degradation in deriving data products from high-resolution C-OPS profiles as a result of incorrectly altering the vertical offset between the pressure transducer and the sensor apertures. The degradation is expressed as the RPD between the results obtained for the original processing parameters with correct offsets versus the subsequent processing results wherein the vertical offset was incorrectly displaced by 1, 2, 4, 8, 16, and 32 cm (as shown using a unique color for each vertical displacement value). The four panels correspond to the degradation analyses in $L_W(\lambda)$ for (a) the blue water type, (b) the green water type, and (c) the red water type, as well as to (d) the degradation in the derived chlorophyll a concentration (using the OC4v5 band ratio algorithm) as a function of the aforementioned water types and the six vertical displacement values.

5.1 Vertical displacements

To begin the analysis, the RPD in the determination of $R_{rs}(\lambda)$ is considered as a function of an increasing size of an artificial displacement, δ , ranging from 1 to 32 cm. The displacements represent potential errors in $L_u(z, \lambda)$ and $E_d(z, \lambda)$ due to the fact that the depth, z , for each light measurement is determined by the pressure transducer at a different horizontal plane than each of the optical sensors, which also differ from each other. The RPD values are computed by first establish-

ing the reference extrapolation intervals, wherein $\delta = 0$ cm. Next, δ is increased and the data are reprocessed using the reference extrapolation intervals, but with the displacement applied to the original data. A 1 % threshold is set for calibration and validation activities or algorithms requiring absolute radiometry (e.g., next-generation mission planning), so biases to within 1 % are considered negligible.

The results for the blue water type (Fig. 4a) show that all displacements have a bias, which means the processing scheme is sufficiently sensitive to detect displacements at the

1 cm scale. For the 1 and 2 cm displacements, all biases are less than 1 %, and for the 4 cm displacement only the 780 nm channel starts to exceed 1 %. For all other displacements, the biases first increase in the NIR and UV domains, and then subsequently in the blue and red regions. Notably, the blue-green domain remains substantially to within 1 % even with a displacement as large as 32 cm (the 32 cm value may seem excessive, but consider the size of a Niskin bottle and the attendant uncertainty in vertical sample location). In the green water type (Fig. 4b), the 2 cm displacement is barely contained within the 1 % threshold, and all displacements first show the greatest sensitivity in the UV followed by the NIR. The reversal to a lower RPD value at 320 nm is caused by the low radiances at this value for which the displacements can cause non-physical results, which are flagged by the processor and ignored. The smallest amount of structure for each displacement curve is in the vicinity of the spectral peak (560 nm). The results for the red water type (Fig. 4c) show that even a 1 cm displacement significantly degrades the UV and blue parts of the domain, such that the 1 % threshold is exceeded. Consequently, the axiom adopted here is that 1 % radiometry requires a 1 cm perspective. The least amount of structure in each displacement curve is associated with the peak in the spectrum (around 683 nm), although when $\delta = 8$ cm the structure around the peak is significant.

Band ratios of $R_{rs}(\lambda)$ are a common parameter for ocean color inversion algorithms, e.g., the ocean color (OC) number 4 (OC4) algorithm is widely used to derive the chlorophyll *a* concentration (O'Reilly et al., 1998). Considering now the absolute percent differences (APD) to provide a more direct estimate of uncertainty, because positive and negative differences do not cancel, the APD in the OC4 version 5 (OC4v5) data product is investigated as a function of the vertical displacement values (Fig. 4d). For the blue and green water types, the effect of the displacement is always less than 3 %. For the red water type, uncertainties rise steadily with increasing displacement but do not surpass 25 % – the current threshold in acceptability (Hooker and Esaias, 1993) – until the displacement is 32 cm.

5.2 Dark offsets and pressure tares

To investigate whether or not the validation of ocean color algorithms based on band ratios is as robust in coastal waters as in the open ocean – which Fig. 4d implies and the literature supports (Bailey et al., 2008) – an additional set of theoretical sensitivity analyses were performed. In these trials, measurements of two types of dark offsets were combined with three types of pressure tares. The dark offsets establish the bias signal for each gain stage for each channel of the light sensors, and the pressure tare provides the bias signal for the ambient atmospheric pressure. Assuming small vertical tilts during deployments (i.e., to within 5°), the vertical distance from the light aperture to the pressure transducer is

nearly constant and easily included in computing the actual depth of each aperture.

Pressure tares are vertical displacements (in water height), which, if misapplied, represent an artificial bias with respect to the actual depth where the light apertures record data. The absence or misapplication of dark offsets also bias the data, especially for the highly attenuated parts of the spectrum that are at low signal amplitude (and, thus, likely measured at high gain where the sensitivity to a bias is greatest). Both biases can be thought of in terms of an artificial brightening or darkening of the observed light measurement with respect to the true in situ value, which is equivalent to inappropriately displacing the light sensors up or down, respectively, in the water column.

When optical sensors are calibrated by the manufacturer, both dark offset and pressure tare measurements are recorded. The pressure tare is referenced to the local barometric pressure, because so-called *absolute* transducers are normally used and such transducers measure the pressure differential from vacuum. When the instrument is transported to the field, it experiences a different atmospheric condition, and barometric pressure differences can be equivalent to many centimeters of water depth. Over the course of a field campaign, differences in barometric pressure changes can induce biases in the depth measurement of several centimeters. Furthermore, pressure transducers and their processing electronics are also affected by temperature changes and may also experience time-related drift. Optical sensors are also affected by temperature and temporal degradation, which primarily affect the dark offsets.

The additional theoretical sensitivity trials presented here also seek to demonstrate the uncertainties that can occur if the practitioner is not vigilant in minimizing avoidable sources of bias associated with dark offsets and pressure tares. In these trials, two types of dark offsets were combined with three types of pressure tares: the dark offsets were either taken from the calibration file (so-called *calibration* darks) or measured in the field on a daily basis by commanding the sensors to step through all gain stages. The pressure tares were either (a) measured in the field each day shortly before data acquisition, (b) determined as a fixed offset for the entire field campaign (in this case from an analysis of meteorological data), or (c) not done at all (a seemingly extreme omission that does occur). This yielded six trials, but one of these is the reference trial, so only five trials are presented for each of the three water types:

1. calibration darks and daily field pressure tare,
2. daily field darks and a fixed pressure tare,
3. calibration darks and a fixed pressure tare,
4. daily field darks and no pressure tare, and
5. calibration darks and no pressure tare.

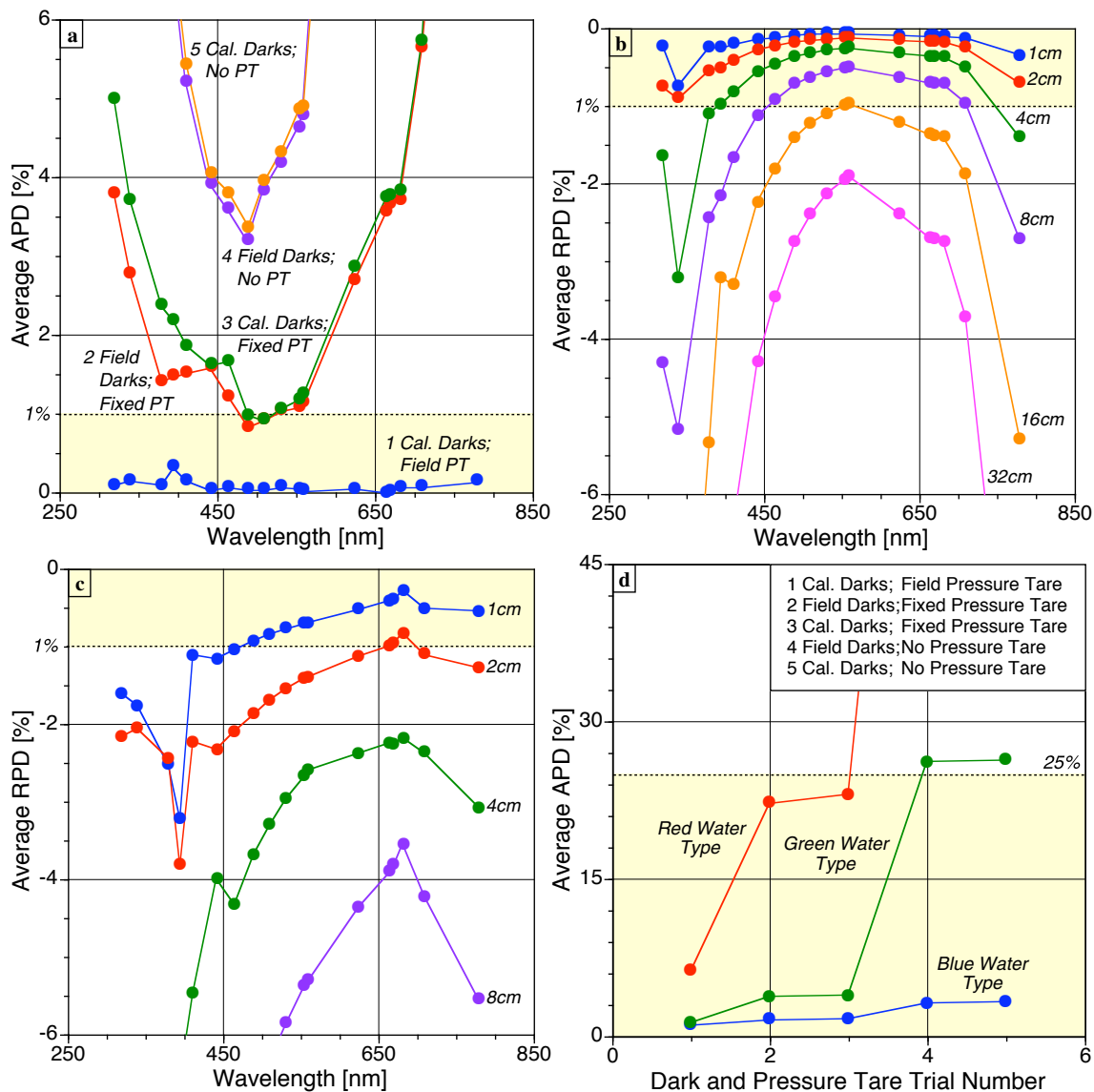


Fig. 5. The degradation in deriving data products from high-resolution C-OPS profiles as a result of incorrectly determining the dark offsets and the pressure tare. The degradation is expressed as the APD between the results obtained for the original processing parameters wherein field dark offsets and field pressure tares were used versus alternatives wherein field dark offsets, calibration darks, a fixed pressure tare, or no pressure tare were used (as shown using a unique color for each of five alternative combinations). The four panels correspond to the degradation analyses in $L_W(\lambda)$ for (a) the blue water type, (b) the green water type, and (c) the red water type, as well as to (d) the degradation in the derived chlorophyll *a* concentration (using the OC4v5 band ratio algorithm) as a function of the aforementioned water types and the five alternatives for dark offsets and pressure tares.

The reference trial was daily field darks and daily field pressure tares.

The results of these trials for the blue water type fall into three groupings in accordance with the pressure tare (Fig. 5a). The only case for which the uncertainties are rather small is when calibration darks are used with a field pressure tare – all other combinations of dark current and pressure tare data collection result in moderate or large uncertainties. The greatest sensitivity is in the NIR and UV domains, followed by the red and blue regions. For the green water

type (Fig. 5b), the use of calibration darks and a field pressure tare causes increasingly large uncertainties in the UV wavelengths in the progression towards shorter wavelengths. The other spectral domains are not significantly affected. Using a fixed pressure tare produces very large uncertainties in the UV and NIR, and large uncertainties in the blue and red spectral domains. Not using a pressure tare results in unacceptably large uncertainties across all wavelengths (and no results are within the y-axis boundaries). The red water type was already shown to be very sensitive, and the only dark

offset and pressure tare trial that actually appears within the plot boundaries is the one for calibration darks and a field pressure tare (Fig. 5c). The results exhibit a rapid increase in uncertainties for wavelengths less than 500 nm, that is, the blue and the UV. The other wavelengths are slightly elevated with respect to the other two water types, but still to within about 0.5 %.

The band ratios of $R_{rs}(\lambda)$ once again mitigate the spectral sensitivities in acquiring AOP data. Although the use of calibration darks rather than field darks in the UV and blue domains for the green and red water types was significant, the effect on OC4v5 is only about 6 % or less (Fig. 5d). The use of fixed pressure tares does not substantially affect the OC4v5 results for the blue and green water types, but it is significant for the red water type. Not using a pressure tare results in a small uncertainty for the blue water type, but it produces unacceptably large uncertainties for the green and red water types (the results are off the plot for the latter). This example of not using a pressure tare for the blue water type should not imply that the blue water type is sufficiently insensitive that the pressure tare can be omitted. It is not unusual for seemingly blue-water sampling to have near-surface complexities (e.g., from an algal bloom or a dust deposition event) such that accurate depths are important.

6 Attenuation classification

In the progression from the open ocean, through the coastal ocean, and into near-shore estuaries and rivers (Fig. 2), the spectral sensitivities – that is, the parts of the spectrum wherein the vertical resolution is important – evolve with the general increase in turbidity as the water depth shallows. The shifting sensitivities, in turn, are convolved with how the signal levels change within the spectral domain (Fig. 4). The sensitivities reveal which spectral regions are radiometrically deep (low attenuation and low sensitivity) and which are radiometrically shallow (high attenuation and high sensitivity). The open ocean is most sensitive in the NIR and UV domains, followed by the blue and red regions. For the coastal ocean, the UV and NIR domains are the most sensitive, followed by the blue and red regions. In the shallow estuaries and rivers, the greatest sensitivity is in the UV and blue, followed by the green and NIR. In all three water types, the domain peak of the spectrum is the most resilient (Fig. 2).

The varying spectral dependence of sensitivity suggests that water type classifications linked to an attenuation or turbidity parameter might be possible, as long as the protocols for acquiring AOP data are strictly followed, as they were for C-OPS during Malina. This logic follows from the original contributions of Jerlov (1951, 1964, and 1976), although a more extensive spectral range is considered here. Furthermore, the larger sensitivity at the end members of the spectral domain (the UV and NIR), as a function of the three water types discussed above (Fig. 4), suggests a parameter

like $K_d(\lambda)$ would be an appropriate choice. From a generalized perspective of responsiveness, changes in the UV part of the spectrum can be considered as absorption dominated and changes in the NIR part as scattering dominated. Consequently, the use of $K_d(320)$ and $K_d(780)$ provides for a simplified depiction of attenuation using proxy variables that mimic aspects of a portrayal based on inherent optical properties (IOPs).

Two advantages of using K_d , especially in turbid waters, are that it can be determined very close to the sea surface (i.e., in very shallow waters) and that it does not require a self-shading correction, whereas an approach based on L_W or R_{rs} does (Gordon and Ding, 1992). A first-order requirement in developing the classification scheme is to demonstrate that the parameters of interest are taken from a part of the water column that is convincingly representative of the optical properties of the water mass that emerge to define the remotely sensed signal. In other words, the parameters of interest should be taken from the same part of the water column that establishes $L_W(\lambda)$. As presented in the companion paper (Antoine et al. 2013; this issue), the determination of the extrapolation intervals uses a bounding condition on the above- and in-water estimates of the global irradiance at null depth that requires the use of calibrated sensors.

Given the multitude of rivers that influence the coastal zone, a scheme that can distinguish finer-scale differences (e.g., one river from its neighbor) is significantly more useful than one that only distinguishes bulk properties (e.g., the open ocean from the coastal ocean). For the Malina data set, it is anticipated that a scheme that can reveal small optical differences in water properties might be useful in revealing whether or not near-ice water masses are different than the neighboring open ocean. The ice is a source of particles and compounds that are released when the ice melts, so the possibility of a finer-scale difference is anticipated.

To test the concept, prior to Malina SuBOPS was used in the fall of 2008 to sample the Gulf of Maine in the area around Portsmouth, New Hampshire. In this field campaign, the SuBOPS profiler was ballasted and trimmed to be as similar to C-OPS as possible, which had just been field commissioned earlier in the year. The coastal region involved multiple rivers, wetlands, near-shore marshes, estuaries, and shallow embayments with connection to the open ocean. The principal watershed drainage that was sampled included Great Bay and Little Bay, the Piscataqua River, and the Merrimack River. Minor watershed drainage included the Saco River, the Kennebec River, and a saltwater marsh. The range in near-surface salinity was 0.1–32.9 PSU, and the range in water depth was 3.7–254.0 m.

The basic water masses for the Gulf of Maine sampling area are presented in Fig. 6 in terms of their $K_d(320)$ versus $K_d(780)$ relationships. Each water mass is presented with separate symbols and color coding, and then major contributors to the observed properties (in terms of the observed dynamic range of the signal) are highlighted with arrows. The

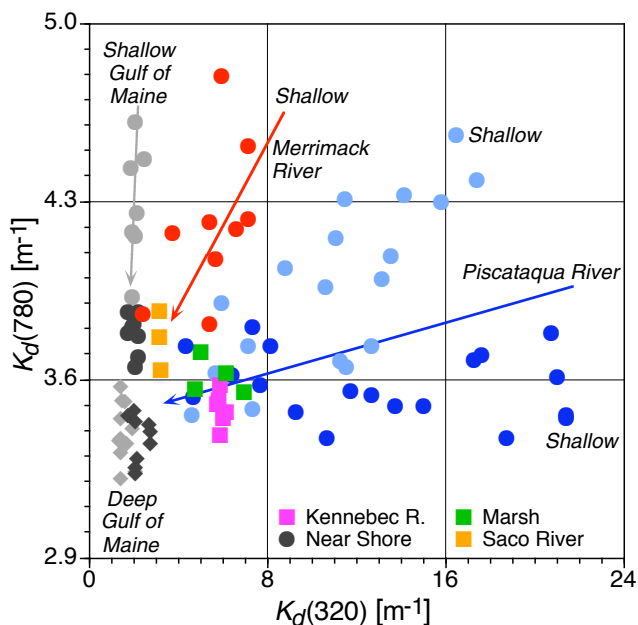


Fig. 6. A plot of $K_d(320)$ versus $K_d(780)$ for the Gulf of Maine sampling done in the vicinity of Portsmouth, New Hampshire. The sampling included the following water masses: an offshore-to-onshore Gulf of Maine transect through the Wilkinson Basin (light gray diamonds), which ended in shallow waters (light gray circles); individual Gulf of Maine deep stations, which are separated into deep (dark gray diamonds) and shallow or near-shore waters (dark gray circles); the Merrimack River (red circles); the Piscataqua River (blue circles) with the major branch of the Piscataqua River (dark blue circles) incorporating Great Bay and Little Bay shown separately (light blue circles); the Saco River (orange squares); the Kennebec River (pink squares); and a coastal marsh (green squares). The overlaid arrows are color coded to the corresponding data sets and show a progression in water properties from shallow head waters (top and right of plot) to deep outflow waters (bottom and left of plot).

latter includes an offshore-to-onshore Gulf of Maine transect through the Wilkinson Basin (light gray diamonds) that included sampling in water depths as shallow as 5.1 m (light gray circles), wherein bottom resuspension was visually discerned. The Piscataqua River, which is the largest river in the study area, is presented with the major branch encapsulating Great Bay and Little Bay with a lighter (blue) color than the main branch (dark blue). Near-shore data collected in Gulf of Maine waters, e.g., very close to islands or geographic features, are distinguished separately as deep-water (dark gray diamonds) and shallow-water (dark gray circles) stations.

The data in Fig. 6 show that major sources of water properties – near-shore terrestrial input encompassing watershed outflow and bottom resuspension – are distinctly identified. The *mixing lines* (denoted by arrows) reveal how the source waters evolve and become part of the open-ocean (deep-water) signal of the Gulf of Maine. The mixing lines converge towards a cluster of points that include the minor

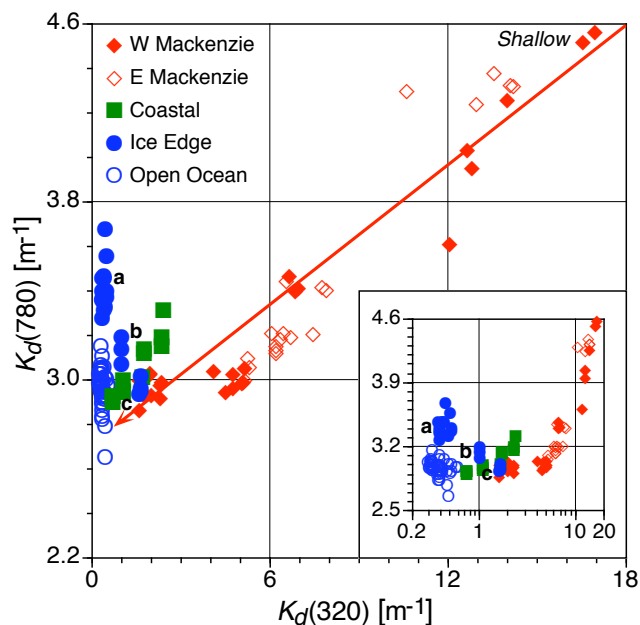


Fig. 7. A plot of $K_d(320)$ versus $K_d(780)$ for the Malina sampling, which was centered around the Mackenzie River outflow, using the same symbols as Fig. 1. The sampling included the following water masses: the open ocean (open blue circles), the western branch of the Mackenzie River (solid red diamonds), the eastern branch of the Mackenzie River (open red diamonds), coastal waters (green squares) and the ice edge (solid blue circles). The latter are further distinguished by the influence of the Mackenzie River plume: (a) no influence; (b) some influence; and (c) the most influence. The overlaid red arrow shows a progression in water properties from shallow waters (top right) to deep waters (bottom left). The inset panel shows the same data with a logarithmic x-axis to improve the clarity of the data with low $K_d(320)$ values.

sources from the Saco River (orange squares), the Kennebec River (pink squares), a coastal marsh (green squares), and near-shore sources of terrestrial inputs (dark gray diamonds and circles). The minor sources surround the periphery of the open-ocean waters of the Gulf of Maine (light gray diamonds). The slopes of the lines for the major sources or the color-coded cluster of points for the minor sources in Fig. 6 establish the generalized relationship between $K_d(320)$ and $K_d(780)$ for each source. Note that the uses of “major” and “minor” denote water volume or the amount of data sampling that was possible; in fact, some so-called minor sources for this analysis might be important sources of a constituent that is not considered here. The principal point is that the $K_d(320)$ and $K_d(780)$ relationships in Fig. 6 are rather uniquely determined in an areal extent bounded by the distribution of sampling within each source. Overlap does occur and is seen to be a function of the variance in defining each source and the convergence of the different sources as they establish the resultant optical properties of the Gulf of Maine, both shallow and deep.

A similar analysis for the Malina data set is shown in Fig. 7, for which the two branches of the Mackenzie River (west and east) are seen to be rather similar and converge with the coastal observations before merging with the open-ocean data. In this on- to offshore transition, the R_{rs} spectral peak starts in the red part of the spectrum (river), shifts to the green (coastal), and then ends in the blue (open ocean). A fifth category representing observations near the ice edge, which have an R_{rs} peak in the blue part of the spectrum like the open ocean, has three different relationships based on the influence of the Mackenzie River plume: (a) no influence; (b) some influence; and (c) the most influence. The data separate convincingly into these respective categories, but, although the coastal category has a peak in the green part of the spectrum, it is not a truly independent category because there is recurring influence on the coastal water type by the Mackenzie River plume.

7 Algorithm derivation

Whether or not $K_d(\lambda)$ can be used to derive a water constituent is evaluated here by using the two spectral end members to form a single parameter, $K_d(320)/K_d(780)$. Across the dynamic range of the open ocean to coastal estuaries and rivers, the numerator can be essentially zero (from a measurement perspective), but the denominator cannot; thus, the ratio as formed is always positive definite. Recalling the desire to be able to classify the diversity of water masses associated with the source waters of coastal watersheds, the mixed coastal environment, and the open ocean, the hypothesis addressed here is whether or not the $K_d(320)/K_d(780)$ ratio can be used to quantify a constituent that is useful to the classification objective and the next-generation perspective. The light absorbance of colored dissolved organic matter (CDOM) has a strong influence on AOPs, with maximum influence in coastal waters (Siegel et al., 2002), and has been successfully derived from in situ and satellite AOP observations (Mannino et al., 2008) and for the Malina data set by Doxaran et al. (2013). Summary details of the seawater analyses used to derive the absorption coefficient of CDOM, $a_{CDOM}(\lambda)$, are presented in the companion paper (Antoine et al., 2013) and in greater detail by Matsuoka et al. (2012).

A secondary advantage with $K_d(\lambda)$, which might be exploited once the approach is established, is that high-quality $K_d(\lambda)$ values do not require a calibrated sensor – the sensor need only be stable over the short time needed to collect the data. This potentially means that coastal monitoring activities involving the flux of a more complex constituent, like CDOM, might be estimated using simpler measurement techniques if there is a satisfactory correlation between the absorption due to CDOM and the attenuation processes captured by the two-channel $K_d(320)/K_d(780)$ ratio. In this study, a_{CDOM} values at 440 nm are used because this is where phytoplankton absorption is maximal. This link is attractive

because much of the remote sensing perspective is also based on the distribution of phytoplankton.

In coastal waters, the parameters being considered here are frequently complex and can exhibit strong spatial and temporal variations. This is especially true in estuaries and near-shore environments that are direct sources of terrestrial inputs to the ocean. Indeed, this significant variability is the reason why there is not a global ocean color algorithm that is as effective for coastal waters as it is for open-ocean waters and why regional empirical algorithms are developed for smaller-scale applications. The initiation of this study is not different in that regard.

The optical data were screened based on the variability observed in the data to only use those individual casts for which (a) there was a close temporal match (to within 60 min in the open ocean and 15 min in shallow waters) between the optical casts and the in-water CDOM analyses, and (b) the highest quality level during processing of the optical data was achieved (three quality levels are determined during the processing based in part on the convergence between the above- and in-water estimates of the global irradiance at null depth). This removed some of the most turbid samples, but nonetheless retained 126 in-water casts out of an original total of 131 possible matchups. Ultimately, two matchups were ignored because they appeared as outliers, so the algorithm was developed using 124 data pairs. The data pairs were not unique, however, because the optical sampling involved the collection of three or more casts per water sampling event, for which there were 40 unique water samples.

The relationship between $K_d(320)/K_d(780)$ and $a_{CDOM}(440)$ for the screened Malina data set is presented in Fig. 8 (the two outliers are the open circles, one atop the other, in the inset panel). The span of horizontal grouping in the individual data clusters is an indication of the amount of variability in the K_d optical properties during the acquisition of the data for each water sample, which are always rather small. The dynamic range in a_{CDOM} covers almost two decades, 0.019–1.025 m^{-1} , with a similar range in $K_d(320)$ of 0.31–17.00 m^{-1} ; the range in $K_d(780)$ is necessarily less and spans 2.82–10.71 m^{-1} . A principal indicator as to the quality of the derived relationship is the coefficient of determination, which indicates that more than 99 % of the variance is explained by the least-squares linear fit, with an RMSE value of 4.2 %. The x-intercept at $y = 0$ is a small positive number (0.05) that is the same order of magnitude as the applicable ratio for pure water, i.e., $K_w(320)/K_w(780) = 0.02$.

8 Discussion and conclusions

To investigate the robustness of the relationship established in Fig. 8, published coastal data from BioPRO and SuB-OPS that have already been used to derive an a_{CDOM} algorithm based on R_{rs} band ratios (Mannino et al., 2008) are

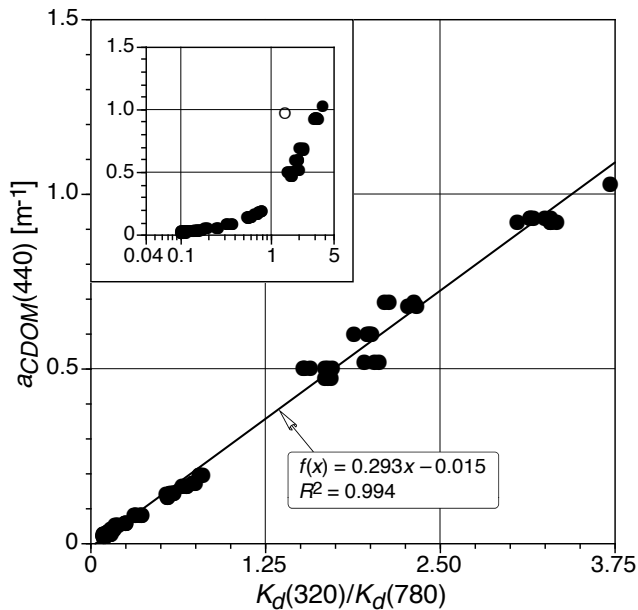


Fig. 8. The relationship between $K_d(320)/K_d(780)$ and $a_{\text{CDOM}}(440)$ for the Malina data set and the resulting linear least-squares fit of the data (solid black line), with the fitting parameters shown bottom right. The inset panel (top left) shows the same data with a logarithmic x-axis to improve the clarity of the data with low $K_d(320)/K_d(780)$ values. The open circles (one atop the other) are two data points that were ignored in the fit because they appear as unexplained outliers.

used to validate the proposed algorithm. The validation data set is from observations made in US coastal waters within the Southern Mid-Atlantic Bight (SMAB) during the period of 2005–2006. The sampling stretched from the Chesapeake Bay to the Delaware Bay with 319 optical profiles collected with contemporaneous water sampling within the upper 5 m of the water column from 59 stations. The latter is a distinguishing feature with respect to the Malina sampling for which almost all of the water samples were taken as surface samples.

To ensure comparability with the C-OPS data used in Fig. 8, in terms of the observed heterogeneity in the data, the BioPRO and SuBOPS data were restricted to sample analyses within 2 m of the surface and a maximum time difference between the optical observations and the seawater sampling of 15 min. The resulting validation data set is composed of 111 data pairs. The equation for the new least-squares linear regression between $a_{\text{CDOM}}(440)$ and the $K_d(320)/K_d(780)$ ratio – now not involving any Malina observations – is $f(x) = 0.292x - 0.023$ with approximately 98 % of the variance explained and an RMSE value of 3.0 %. The dynamic range of the validation data set is not as large as the Malina data, although it spans a little more than an order of magnitude for both variables of interest: $a_{\text{CDOM}}(440)$ ranges

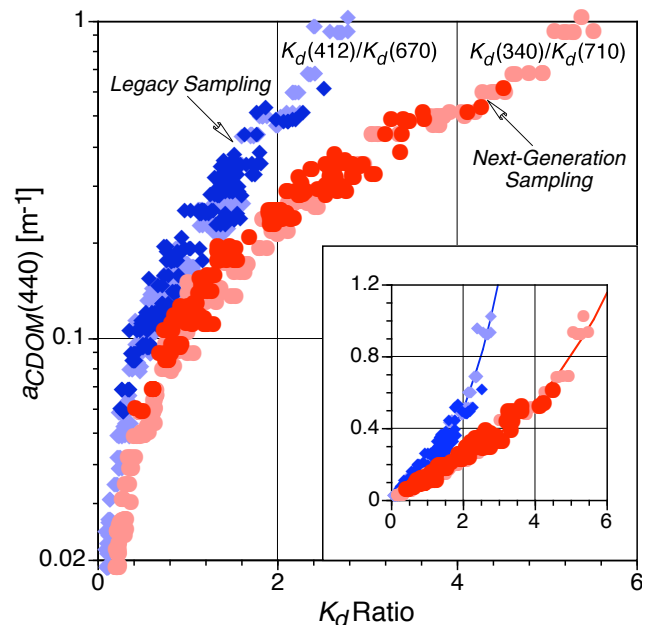


Fig. 9. The relationship between two alternative K_d ratios as a function of $a_{\text{CDOM}}(440)$ for the Malina (light symbols) and SMAB (dark symbols) data set. The $K_d(340)/K_d(710)$ ratio is shown in red and the $K_d(412)/K_d(670)$ ratio in blue. A logarithmic y-axis is used to clarify the data with low $a_{\text{CDOM}}(440)$ values. The inset panel (bottom right) shows the same data with a linear y-axis, so the functional relationships – in this case approximated by third-order polynomials – are easier to discern.

from approximately 0.04 to 0.45 m^{-1} and $K_d(320)/K_d(780)$ ranges from approximately 0.1 to 1.6.

The validation data used a more restrictive temporal matchup requirement of 15 min or less, because the sampling procedures with these data exhibited greater variance (on average), e.g., time differences between the optical observations and seawater sampling sometimes exceeded 90 min. Restricting the Malina data to a 15 min or less sampling time difference does not change the derived algorithm (Fig. 8) at the adopted precision: the linear least-squares regression is $f(x) = 0.293x - 0.015$ with more than 99 % of the variance explained and an RMSE value of 3.6 %. The principal reason why the temporal restriction is not important to the Malina data is that sampling almost always occurred within a 15 min time span, and the few times this did not occur, the sampling was in deeper waters that evolved rather slowly.

The close agreement between the two derivations of the $a_{\text{CDOM}}(440)$ algorithm using data from disparate geographic locations representing significantly different ecosystems and watersheds suggests that the algorithm might have wider applicability than to a specific region. To test additional aspects of the robustness of using K_d end members as the basis for a CDOM algorithm, two other spectral combinations are evaluated. The first uses slightly different wavelengths that are within the same spectral domain as the original algorithm

and in keeping with a next-generation scientific perspective (i.e., the UV and NIR wavelengths), and the second uses substantially different wavelengths that are in keeping with the present-generation scientific perspective (i.e., blue and red wavelengths).

The two alternative wavelength combinations are based on $K_d(340)/K_d(710)$ and $K_d(412)/K_d(670)$. The relationship of the two alternative ratios with respect to $a_{CDOM}(440)$ is presented in Fig. 9. In both cases, the Malina and SMAB data exhibit close agreement and both yield smoothly varying functional relationships, although they are not linear. The figure shows fits based on third-order polynomials, but quadratic functions explain a similar amount of variance: over 94 % for the former and over 95 % for the latter. Note that the use of alternative wavelengths alters the optical dynamic range in terms of the K_d ratio; the $K_d(340)/K_d(710)$ data have a larger dynamic range than the $K_d(320)/K_d(780)$ data (Fig. 8), while both of them have a larger dynamic range than the $K_d(412)/K_d(670)$ data.

The strongly correlated functional forms presented in Figs. 8 and 9 are a direct result of tightly coupling the derivation of the near-surface AOP parameters with contemporaneous near-surface seawater sampling. The tight coupling is a result of (a) screening and filtering the CDOM data both temporally and vertically to ensure it matched as close in space and time to the extrapolation interval used to derive the AOP data products as possible, and (b) collecting in situ light measurements with unprecedented vertical resolution such that high-quality data products can be produced very close to the sea surface.

An immediate benefit of this approach was summarized in the theoretical sensitivity trials (Figs. 4 and 5), wherein even small diversions from strict adherence to the Protocols were seen at the 1 % and 1 cm level in the absolute radiometry – most notably at the end members of the spectrum – but were substantially not expressed in the band ratios until the diversions became very large or the optical complexity became significant (as defined both in terms of the light spectrum and the water type). The sensitivity of the spectral end members revealed how the different source waters in a coastal environment can be uniquely characterized and two-dimensionally mapped in terms of the $K_d(\lambda)$ end-member values. The fine-scale level of discrimination this afforded showed how oceanic waters close to the ice edge are notably different from the open ocean (Fig. 7).

Finally, ratios of $K_d(\lambda)$ spectral end members in the UV and NIR, which were presented as proxy variables for absorption and scattering, respectively, were found to correlate with $a_{CDOM}(440)$ with sufficient robustness to establish an algorithm to derive $a_{CDOM}(440)$ from K_d with high accuracy (approximately 98 % of the variance explained and an RMSE value of 3.0 % for temporally and spatially screened data). The derivation of $a_{CDOM}(440)$ from the $K_d(320)/K_d(780)$ ratio represents a novel solution to a problem that has been discussed in the literature, albeit primarily with a focus on

the visible domain (e.g., Pierson et al., 2008) and not on the UV and NIR domains, wherein it is frequently more difficult to derive high-quality data products.

This study was motivated, in part, by the programmatic science questions posed in Sect. 1, in order to create new tools that might allow researchers to describe environmental changes in ecosystems using new algorithms, as well as simpler and less-expensive technologies than presently used. For instance, deploying a two-band light instrument is much simpler and less expensive than collecting seawater for analysis. Monitoring the transitions of CDOM pools between coastal and oceanic habitats over large geographical distributions is a more tractable problem with less complex and inexpensive observing equipment (i.e., a two-channel radiometer). Equally intriguing is the potential to use simple optical instruments to understand how pollutants will be expressed in the relationships presented here and whether or not alternative band sets will provide more-sensitive measures of pollutants.

Acknowledgements. Much of the next-generation perspective presented here was developed as part of the calibration and validation activities of the SeaWiFS, SIMBIOS, and MODIS projects, as well as the Malina optical team. The high level of success achieved in the field work for those activities established a foundation of understanding that was the direct consequence of contributions from many individuals who contributed unselfishly to the work involved (e.g., calibration, acquisition, processing, and sampling). The scientists include (alphabetically) D. Antoine, J. Brown, C. Dempsey, S. Maritorena, and G. Zibordi; their dedicated contributions are gratefully acknowledged.

Edited by: W. Miller

References

- Antoine, D., d'Ortenzio, F., Hooker, S. B., Bécu, G., Gentili, B., Tailliez, D., and Scott, A. J.: Assessment of uncertainty in the ocean reflectance determined by three satellite ocean color sensors (MERIS, SeaWiFS and MODIS-A) at an offshore site in the Mediterranean Sea (BOUSSOLE project), *J. Geophys. Res.*, 113, C07013, doi:10.1029/2007JC004472, 2008.
- Antoine, D., Hooker, S. B., Bélanger, S., Matsuoka, A., and Babin, M.: Apparent optical properties of the Canadian Beaufort Sea – Part 1: Observational overview and water column relationships, *Biogeosciences*, 10, 4493–4509, doi:10.5194/bg-10-4493-2013, 2013.
- Bailey, S. W., Hooker, S. B., Antoine, D., Franz, B. A., and Werdell, P. J.: Sources and assumptions for the vicarious calibration of ocean color satellite observations, *Appl. Optics*, 47, 2035–2045, 2008.
- Bernhard, G., Booth, C. R., Morrow, J. H., and Hooker, S. B.: Biospherical Shadowband Accessory for Diffuse Irradiance (BioSHADE): a marine shadowband and gps accessory, in: Advances in Measuring the Apparent Optical Properties (AOPs) of Optically Complex Waters, NASA Tech. Memo. 2010–215856,

- by: Morrow, J. H., Hooker, S. B., Booth, C. R., Bernhard, G., Lind, R. N., and Brown, J. W., NASA Goddard Space Flight Center, Greenbelt, Maryland, 51–60, 2010.
- Booth, C. R., Morrow, J. H., Lind, R. N., and Hooker, S. B.: Development of the microradiometer, in: *Advances in Measuring the Apparent Optical Properties (AOPs) of Optically Complex Waters*, NASA Tech. Memo. 2010–215856, by: Morrow, J. H., Hooker, S. B., Booth, C. R., Bernhard, G., Lind, R. N., and Brown, J. W., NASA Goddard Space Flight Center, Greenbelt, Maryland, 27–41, 2010.
- Clark, D., Gordon, H. R., Voss, K. J., Ge, Y., Broenkow, W., and Trees, C.: Validation of atmospheric correction over the oceans, *J. Geophys. Res.*, 102, 17209–17217, 1997.
- Cota, G. F., Wang, J., and Comiso, J.C.: Transformation of global satellite chlorophyll retrievals with a regionally tuned algorithm, *Remote Sens. Environ.*, 90, 373–377, 2004.
- Doxaran, D., Ehn, J., Bélanger, S., Matsuoka, A., Hooker, S., and Babin, M.: Optical characterisation of suspended particles in the Mackenzie River plume (Canadian Arctic Ocean) and implications for ocean colour remote sensing, *Biogeosciences*, 9, 3213–3229, doi:10.5194/bg-9-3213-2012, 2012.
- Gordon, H. R. and Ding, K.: Self shading of in-water optical instruments, *Limnol. Oceanogr.*, 37, 491–500, 1992.
- Hlaing, S., Harmel, T., Ibrahim, A., Ioannou, I., Tonizzo, A., Gileron, A., and Ahmed, S.: Validation of ocean color satellite sensors using coastal observational platform in Long Island Sound, *Proc. SPIE*, 7825, 782504, doi:10.1117/12.865123, 2010.
- Hooker, S. B.: The Telescoping Mount for Advanced Solar Technologies (T-MAST), in: *Advances in Measuring the Apparent Optical Properties (AOPs) of Optically Complex Waters*, NASA Tech. Memo. 2010–215856, edited by: Morrow, J. H., Hooker, S. B., Booth, C. R., Bernhard, G., Lind, R. N., and Brown, J. W., NASA Goddard Space Flight Center, Greenbelt, Maryland, 66–71, 2010.
- Hooker, S. B. and Brown, J. W.: Processing of Radiometric Observations of Seawater using Information Technologies (PROSIT): In-Water User Manual, NASA Tech. Memo., NASA Goddard Space Flight Center, Greenbelt, Maryland, in preparation, 2013.
- Hooker, S. B. and Esaias, W. E.: An overview of the SeaWiFS project, *Eos T. Am. Geophys. Un.*, 74, 241–246, 1993.
- Hooker, S. B. and Maritorena, S.: An evaluation of oceanographic radiometers and deployment methodologies, *J. Atmos. Ocean. Tech.*, 17, 811–830, 2000.
- Hooker, S. B. and McClain, C. R.: The calibration and validation of SeaWiFS data, *Prog. Oceanogr.*, 45, 427–465, 2000.
- Hooker, S. B. and Zibordi, G.: Platform perturbations in above-water radiometry, *Appl. Optics*, 44, 553–567, 2005.
- Hooker, S. B., McClain, C. R., Firestone, J. K., Westphal, T. L., Yeh, E.-N., and Ge, Y.: The SeaWiFS Bio-Optical Archive and Storage System (SeaBASS), Part 1, NASA Tech. Memo. 104566, Vol. 20, edited by: Hooker, S. B. and Firestone, E. R., NASA Goddard Space Flight Center, Greenbelt, Maryland, 40 pp., 1994.
- Hooker, S. B., Zibordi, G., Berthon, J.-F., Bailey, S. W., and Pietras, C. M.: The SeaWiFS Photometer Revision for Incident Surface Measurement (SeaPRISM) Field Commissioning, NASA Tech. Memo. 2000–206892, Vol. 13, edited by: Hooker, S. B. and Firestone, E. R., NASA Goddard Space Flight Center, Greenbelt, Maryland, 24 pp., 2000.
- Hooker, S. B., Zibordi, G., Berthon, J.-F., D’Alimonte, D., Maritorena, S., McLean, S., and Sildam, J.: Results of the Second SeaWiFS Data Analysis Round Robin, March 2000 (DARR-00), NASA Tech. Memo. 2001–206892, Vol. 15, edited by: Hooker, S. B. and Firestone, E. R., NASA Goddard Space Flight Center, Greenbelt, Maryland, 71 pp., 2001.
- Hooker, S. B., Lazin, G., Zibordi, G., and McLean, S.: An evaluation of above- and in-water methods for determining water-leaving radiances, *J. Atmos. Ocean. Tech.*, 19, 486–515, 2002.
- Hooker, S. B., Zibordi, G., Berthon, J.-F., and Brown, J. W.: Above-water radiometry in shallow, coastal waters, *Appl. Optics*, 43, 4254–4268, 2004.
- Hooker, S. B., McClain, C. R., and Mannino, A.: NASA Strategic Planning Document: A Comprehensive Plan for the Long-Term Calibration and Validation of Oceanic Biogeochemical Satellite Data, NASA Special Pub. 2007–214152, NASA Goddard Space Flight Center, Greenbelt, Maryland, 31 pp., 2007.
- Hooker, S. B., Morrow, J. H., and Brown, J. W.: The Biospherical Surface Ocean Reflectance System (BioSORS), in: *Advances in Measuring the Apparent Optical Properties (AOPs) of Optically Complex Waters*, NASA Tech. Memo. 2010–215856, edited by: Morrow, J. H., Hooker, S. B., Booth, C. R., Bernhard, G., Lind, R. N., and Brown, J. W., NASA Goddard Space Flight Center, Greenbelt, Maryland, 8–16, 2010a.
- Hooker, S. B., Lind, R. N., Morrow, J. H., and Brown, J. W.: The Submersible Biospherical Optical Profiling System (SuB-OPS), in: *Advances in Measuring the Apparent Optical Properties (AOPs) of Optically Complex Waters*, NASA Tech. Memo. 2010–215856, edited by: Morrow, J. H., Hooker, S. B., Booth, C. R., Bernhard, G., Lind, R. N., and Brown, J. W., NASA Goddard Space Flight Center, Greenbelt, Maryland, 17–26, 2010b.
- Hooker, S. B., Bernhard, G., Morrow, J. H., Booth, C. R., Comer, T., Lind, R. N., and Quang, V.: Optical Sensors for Planetary Radiant Energy (OSPREy): Calibration and Validation of Current and Next-Generation NASA Missions, NASA Tech. Memo. 2012–215872, NASA Goddard Space Flight Center, 117 pp., Greenbelt, Maryland, 2012.
- Jerlov, N. G.: *Optical Studies of Ocean Water*, Rept. Swedish Deep-Sea Exped. 1947–1948, 3, 73–97, 1951.
- Jerlov, N. G.: *Optical Classification of Ocean Water*, in: *Physical Aspects of Light in the Sea*, University of Hawaii Press, Honolulu, Hawaii, 45–49, 1964.
- Jerlov, N. G.: *Marine Optics*, Elsevier Scientific Publishing Company, Amsterdam, Netherlands, 231 pp., 1976.
- Joint Global Ocean Flux Stud: JGOFS Core Measurements Protocols, JGOFS Report No. 6, Scientific Committee on Oceanic Research, Bergen, Norway, 40 pp., 1991.
- Mannino, A., Russ, M. E., and Hooker, S. B.: Algorithm development and validation for satellite-derived distributions of DOC and CDOM in the US Middle Atlantic Bight, *J. Geophys. Res.*, 113, C07051, doi:10.1029/2007JC004493, 2008.
- Matsuoka, A., Bricaud, A., Benner, R., Para, J., Sempéré, R., Prieur, L., Bélanger, S., and Babin, M.: Tracing the transport of colored dissolved organic matter in water masses of the Southern Beaufort Sea: relationship with hydrographic characteristics, *Biogeosciences*, 9, 925–940, doi:10.5194/bg-9-925-2012, 2012.
- McClain, C., Hooker, S., Feldman, G., and Bontempi, P.: Satellite data for ocean biology, biogeochemistry, and climate research,

- Eos T. Am. Geophys. Un., 87, 337–343, 2006.
- Morel, A. and Prieur, L.: Analysis of variations in ocean color, *Limnol. Oceanogr.*, 22, 709–722, 1977.
- Morrow, J. H., Hooker, S. B., Bernhard, G., and Lind, R. N.: Scalable Hydro-optical Applications for Light Limited Oceanography (SHALLO), in: *Advances in Measuring the Apparent Optical Properties (AOPs) of Optically Complex Waters*, NASA Tech. Memo. 2010–215856, edited by: Morrow, J. H., Hooker, S. B., Booth, C. R., Bernhard, G., Lind, R. N., and Brown, J. W., NASA Goddard Space Flight Center, Greenbelt, Maryland, 60–65, 2010a.
- Morrow, J. H., Booth, C. R., Lind, R. N., and Hooker, S. B.: The Compact-Optical Profiling System (C-OPS), in: *Advances in Measuring the Apparent Optical Properties (AOPs) of Optically Complex Waters*, NASA Tech. Memo. 2010–215856, edited by: Morrow, J. H., Hooker, S. B., Booth, C. R., Bernhard, G., Lind, R. N., and Brown, J. W., NASA Goddard Space Flight Center, Greenbelt, Maryland, 42–50, 2010b.
- Mueller, J. L.: Overview of measurement and data analysis protocol, in: *Ocean Optics Protocols for Satellite Ocean Color Sensor Validation, Revision 2*, NASA Tech. Memo. 2000–209966, edited by: Fargion, G. S. and Mueller, J. L., NASA Goddard Space Flight Center, Greenbelt, Maryland, 87–97, 2000.
- Mueller, J. L.: Overview of measurement and data analysis protocols, in: *Ocean Optics Protocols for Satellite Ocean Color Sensor Validation, Revision 3, Volume 1*, NASA Tech. Memo. 2002–210004/Rev3–Vol1, edited by: Mueller, J. L. and Fargion, G. S., NASA Goddard Space Flight Center, Greenbelt, Maryland, 123–137, 2002.
- Mueller, J. L.: Overview of measurement and data analysis methods, in: *Ocean Optics Protocols for Satellite Ocean Color Sensor Validation, Revision 4, Volume III: Radiometric Measurements and Data Analysis Protocols*, NASA Tech. Memo. 2003–211621/Rev4–Vol.III, edited by: Mueller, J. L., Fargoin, G. S., and McClain, C.R., NASA Goddard Space Flight Center, Greenbelt, Maryland, 1–20, 2003.
- Mueller, J. L. and Austin, R. W.: Ocean optics protocols for SeaWiFS validation, NASA Tech. Memo. 104566, Vol. 5, edited by: Hooker, S. B. and Firestone, E. R., NASA Goddard Space Flight Center, Greenbelt, Maryland, 43 pp., 1992.
- Mueller, J. L. and Austin, R. W.: Ocean optics protocols for SeaWiFS validation, Revision 1, NASA Tech. Memo. 104566, Vol. 25, edited by: Hooker, S. B., Firestone, E. R., and Acker, J. G., NASA Goddard Space Flight Center, Greenbelt, Maryland, 66 pp., 1995.
- National Aeronautics and Space Administration: Responding to the Challenge of Climate and Environmental Change: NASA's Plan for a Climate-Centric Architecture for Earth Observations and Applications from Space, National Aeronautics and Space Administration, Washington, DC, 48 pp., 2010.
- National Research Council: Earth Science and Applications from Space: National Imperatives for the Next Decade and Beyond, The National Academies, Washington, DC, 456 pp., 2007.
- O'Reilly, J. E., Maritorena, S., Mitchell, B. G., Siegel, D. A., Carder, K. L., Garver, S. A., Kahru, M., and McClain, C.: Ocean color chlorophyll algorithms for SeaWiFS, *J. Geophys. Res.*, 103, 24937–24953, 1998.
- Pierson, D. C., Kratzer, S., Strömbeck, N., and Håkansson, B.: Relationship between the attenuation of downwelling irradiance at 490 nm with the attenuation of PAR (400 nm–700 nm) in the Baltic Sea, *Remote Sens. Environ.*, 112, 668–680, 2008.
- Siegel, D. A., Maritorena, S., Nelson, N. B., Hansell, D. A., and Lorenzi-Kayser, M.: Global distribution and dynamics of colored dissolved and detrital organic materials, *J. Geophys. Res.*, 107, 3228, doi:10.1029/2001JC000965, 2002.
- Smith, R. C. and Baker, K. S.: The analysis of ocean optical data, in: *Ocean Optics VII*, edited by: Blizard, M., *Proc. SPIE*, 478, 119–126, 1984.
- Wang, J. and Cota, G. F.: Remote-sensing reflectance in the Beaufort and Chukchi seas: observations and models, *Appl. Optics*, 42, 2754–2765, 2003.
- Zibordi, G., Berthon, J.-F., Doyle, J. P., Grossi, S., van der Linde, D., Targa, C., and Alberotanza, L.: Coastal Atmosphere and Sea Time Series (CoASTS), Part 1: A Tower-Based Long-Term Measurement Program, NASA Tech. Memo. 2002–206892, Vol. 19, edited by: Hooker, S. B. and Firestone, E. R., NASA Goddard Space Flight Center, Greenbelt, Maryland, 29 pp., 2002.
- Zibordi, G., Mélin, F., Hooker, S. B., D'Alimonte, D., and Holben, B.: An autonomous above-water system for the validation of ocean color radiance data, *IEEE T. Geosci. Remote*, 42, 401–415, 2004.